Check for updates

Geophysical Research Letters

RESEARCH LETTER
10.1029/2026GL125585

A Sustained High Growth Regime After Collapse of the Arctic Sea Ice Volume Feedback

B. Mellor[1], **M. Tsamados**[1], **H. Heorton**[2], **P. R. Holland**[3], **and C. Brierley**[2]

[1]Department of Earth Sciences, University College London, London, UK, [2]Department of Geography, University College London, London, UK, [3]British Antarctic Survey, Cambridge, UK

Key Points:

- A 29 years record of Arctic sea ice growth is produced from thickness, concentration and drift retrievals using a volume budget
- Winter growth underwent an upward regime shift around the 2007 record minimum into a high-intensity state
- This shift marks the collapse of the negative volume feedback toward internally variable growth that is weakly tied to atmospheric forcing

Supporting Information:

Supporting Information may be found in the online version of this article.

Correspondence to:

B. Mellor,
benjamin.mellor.24@ucl.ac.uk

Citation:

Mellor, B., Tsamados, M., Heorton, H., Holland, P. R., & Brierley, C. (2026). A sustained high growth regime after collapse of the Arctic sea ice volume feedback. *Geophysical Research Letters*, *53*, e2026GL125585. https://doi.org/10.1029/2026GL125585

Received 17 JUL 2026
Accepted 3 NOV 2026

Author Contributions:

Conceptualization: B. Mellor, M. Tsamados, P. R. Holland
Formal analysis: B. Mellor, H. Heorton
Funding acquisition: B. Mellor
Investigation: M. Tsamados, H. Heorton, P. R. Holland, C. Brierley
Methodology: B. Mellor, M. Tsamados
Software: B. Mellor, H. Heorton
Supervision: M. Tsamados, C. Brierley
Visualization: B. Mellor, H. Heorton
Writing – original draft: B. Mellor
Writing – review & editing: M. Tsamados, H. Heorton, P. R. Holland, C. Brierley

© 2026 The Author(s). Geophysical Research Letters published by Wiley Periodicals LLC on behalf of American Geophysical Union.
This is an open access article under the terms of the Creative Commons Attribution License, which permits use, distribution and reproduction in any medium, provided the original work is properly cited.

Abstract We investigate changing Arctic sea ice growth behavior by synthesizing 29 years (1994–2023) of remote sensing products into a sea ice volume budget. By resolving dynamic and thermodynamic terms, we reveal a regime change in growth. Arctic sea ice has undergone a 1,077 (±259) km^3 increase in mean winter growth following the 2007/08 winter. Before 2007, the volume of survived summer ice explained 62.5% of seasonal winter growth ($p < 0.001$), a strong negative feedback consistent with prior understanding. This feedback collapsed after 2007. Basin growth has since decoupled from snow depth and sea surface temperature, retaining a link only to air temperature since 2014, which suggests a regime in which high internal variability and regional thickness distributions govern basin-wide growth rather than any single forcing. This observational record resolves growth regimes that shorter records cannot separate, and serves as a benchmark for CMIP7 assessment.

Plain Language Summary Arctic sea ice decline is a key cryosphere response to climate change. It is both melting much more than it used to in the summer, and growing much more than it used to in the winter as a compensating feedback. By using three decades of satellite records (1994–2023), we track how sea ice growth has changed by measuring the change in volume due to thermodynamics. Growth increased by 1,077 cubic kilometers on average after 2007. Because thick ice grows less easily, the amount of ice that survives each summer strongly predicts winter growth, the negative feedback of thin-ice. However, after 2007, this basin-wide relationship has collapsed. More surprisingly, ocean-atmosphere controls such as ocean temperature have disconnected from ice growth. Instead, basin ice growth is driven by rapidly growing thin ice, and is weakly affected by air temperature. Our 29-year record provides an extended observational benchmark to test growth in climate models, and reframes our understanding of what controls Arctic sea ice in a warming world.

1. Introduction

The decline of Arctic sea ice is a key cryosphere response to anthropogenic climate change (Serreze, 2011; Winton, 2006). The Arctic has experienced a September sea ice volume (SIV) ablation of ≈10,000 km^3 from the 1990s to 2010 (Gascard et al., 2019). In 2007, a record minimum for sea ice extent (Stern, 2025; Stroeve et al., 2008) and a step-change in sea ice thickness (SIT) decline occurred (Sumata et al., 2023). Since then, both extent and thickness have stabilized (England et al., 2025). The causes of this period of decline and subsequent stabilization are thought of as a confluence of both anthropogenic forcings; increased atmospheric and oceanic heat content, paired with the internal variability of the Arctic sea ice system and the associated feedback mechanisms (Massonnet et al., 2018; Notz & Bitz, 2017).

A key stabilizing mechanism is the thin-ice growth feedback, whereby thinner ice allows greater conductive heat flux and therefore faster ice growth (Hibler, 1979; Nakawo & Sinha, 1981). Climate model sensitivity studies (Petty et al., 2018; Stroeve et al., 2018), and CMIP5 ensembles suggest that non-linear sea ice growth, via the introduction of thin ice, is a key stabilizing mechanism in sea ice decline (Massonnet et al., 2018). Thinner ice is also weaker, enhancing lead formation and winter ice growth within open-water fractions (Mackie et al., 2020; Von Albedyll et al., 2022). Conversely, this ease of fracturing also drives ocean warming by enhancing the ice-albedo feedback during summer months (Bitz & Roe, 2004; Lang et al., 2017), which then dampens volume recovery mechanisms through enhanced ocean heat content and long-wave radiative balance changes (Lim et al., 2022; Notz & Stroeve, 2018; Pollock et al., 2026). Sea ice drift speed has been increasing at 9(±1.9)% per decade, and follows the observed thickness decline of 16.5% per decade (Kwok, 2010; Rampal et al., 2009). Drift

19448007, 2026, 22, Downloaded from https://agupubs.onlinelibrary.wiley.com/doi/10.1029/2026GL125585 by NICE, National Institute for Health and Care Excellence, Wiley Online Library on [19/11/2026]. See the Terms and Conditions (https://onlinelibrary.wiley.com/terms-and-conditions) on Wiley Online Library for rules of use; OA articles are governed by the applicable Creative Commons License

acceleration has increased fracturing, amplified the sea-ice albedo feedback and accelerated summer melt (Rampal et al., 2009). Exploration of these feedbacks on a pan-Arctic scale has been limited to modeling studies (e.g., Keen et al., 2021; Petty et al., 2018; Stroeve et al., 2018), or spatio-temporally limited observational studies (Sumata et al., 2023; West et al., 2020). Remote sensing offers the spatio-temporal scope needed for investigations of pan-Arctic sea ice processes in the real world.

Following the launch of Cryosat-2 (CS2) in 2010, a period of mature radar altimetry SIT retrievals began, enabling assessments of Arctic SIV for 15+ years. Recent advances in retrieval algorithms have enabled the first CS2 aligned retrievals of SIT, integrating the ERS-1, ERS-2 and Envisat thickness records to the winter of 1994 (Bocquet et al., 2023, 2024). Ricker et al. (2021) produced a regional SIV budget utilizing Envisat and CS2, and identified the contribution of ocean heat content to limiting winter growth in the European sector. Yet, this record begins in 2002. By extending this framework to 1994, the first multi-decadal analysis of Arctic winter SIV process changes is possible.

In this study we produce a long-term pan-Arctic SIV budget and decompose the SIV change into dynamic and thermodynamic processes over the period of 1994–2023 to track how winter growth has responded to climate variability. We first establish the negative thin-ice feedback and ice-ocean-atmosphere interactions, and then perform 10 years rolling correlations to test their stationarity. This reveals a basin-wide decoupling in volume feedback, as well as wider changes in ice-atmosphere-ocean interactions. Finally, we provide a robust observational basis for model assessment (Fox-Kemper et al., 2026).

2. Methodology

We use the method of Heorton et al. (2025). The volume V is the integration of thickness, concentration, and grid cell area each with a ± 1 day window. The volume change with respect to time is known as the intensification. Intensification for a grid cell is both dynamic and thermodynamic. By expanding the dynamic term into the contribution of advection *Adv* and divergent *Div* components, the thermodynamic component (melt or growth) can be computed as a residual *Res*.

$$\underbrace{\frac{dV}{dt}}_{Int} = \underbrace{-\mathbf{u}\cdot\nabla V}_{Adv} - \underbrace{V(\nabla\cdot\mathbf{u})}_{Div} + \underbrace{\mathcal{E}}_{Res} \tag{1}$$

The terms *Int*, *Adv*, *Div* are calculated numerically using a second-order central finite difference scheme. The uncertainty of thickness and drift propagates through the full components of the calculus in Equation 1. By assuming perfect spatial autocorrelation ($\rho \rightarrow 1$), and 12-day decorrelation timescale, we provide a *worst-case* uncertainty quantification, ensuring that our results bound the accuracies of the multi-sensor data sources. The dynamic terms depend on the choice of drift product through $\mathbf{u}$, so we perform the budget with both OSISAF and Pathfinder velocity products. The resultant basin-wide *Res* anomaly has a mean absolute error of 19 cm, heightened in high drift-variance export regions such as the Fram Strait (89 cm), see Supporting Information S1.

2.1. Data Products

The longest term SIT product available is the aligned ERS-1 (1994–1996), ERS-2 (1996–2004), Envisat (2004–2012) and CryoSat-2 (2012+) retrievals of SIT by Bocquet et al. (2024). The thickness shows good agreement with in situ validation schemes such as Operation Ice Bridge (Bocquet et al., 2023). *SIT* is an altimetric measurement, with ensemble uncertainty drawn from freeboard and snow density distributions (Bocquet et al., 2023, 2024), that are propagated into the product and supplied as σ_{h_i}. Two constraints follow from the multi-sensor fusion performed by Bocquet et al. (2024). First, the record is restricted to the winter months (ONDJFM) because summer melt ponds disrupt the altimetry freeboard retrieval pipeline (Dawson et al., 2022; Landy et al., 2022). Second, coverage to 81.5°N excludes a portion of the Central Arctic known as the pole-hole, because pre-CS2 satellites orbited at a lower inclination. The impacts of an extended pole-hole are described in Section 3.1 and Supporting Information S1.

We also produce a local level proxy uncertainty from the AWI CS2 SIT record by regressing the thickness $h_{(i,j)}$ upon the uncertainty $h_{\mathrm{Err}(i,j)}$ (Hendricks et al., 2021). Because of the length of CS2 thickness record we omit observed changes in Arctic snowfall, salinity, roughness, and moisture patterns (Edel et al., 2020; Landy

19448007, 2026, 22, Downloaded from https://agupubs.onlinelibrary.wiley.com/doi/10.1029/2026GL125585 by NICE, National Institute for Health and Care Excellence, Wiley Online Library on [19/11/2026]. See the Terms and Conditions (https://onlinelibrary.wiley.com/terms-and-conditions) on Wiley Online Library for rules of use; OA articles are governed by the applicable Creative Commons License

et al., 2020; Screen & Simmonds, 2012; Willatt et al., 2023), all of which are known to affect Ku-band radar altimetry (Nab et al., 2023). Refer to Supporting Information S1 for uncertainty information.

We use the NASA Team Daily product (Cavalieri et al., 1984, 1997), selected for low bias (+0.9%) and its 25 × 25 km polar-stereographic grid (Kern et al., 2019). A sole SIC product is used because the contribution of concentration to budget variance is negligible over the winter. See Section S2 in Supporting Information S1.

Two sea ice drift products are used to test the sensitivity of the volume budgeting method. They are the OSISAF-405 Global Low Resolution Sea Ice Drift found on a 62.5 km polar stereographic grid (Lavergne & Down, 2023). OSISAF-405 applies an independent algorithm to passive-microwave imagery (SSM/I, SSMIS, AMSR-E, AMSR2) to track drift, which is supplemented in the summer by a free-drift model forced by ERA5 10 m components. However, OSISAF-405 only extends until December 2020, so we apply it to this period only. Second, we use the v4 Polar Pathfinder Sea Ice Motion Vectors which combines passive-microwave feature tracking (SMMR, SSM/I, SSMIS, AMSR-E) with free-drift models forced by NCEP/NCAR 10 m winds (Tschudi et al., 2020). We find the drift vector product to be of second-order importance to thickness (Section S2 in Supporting Information S1).

Growth season (ONDJFM) atmospheric and oceanic variables—2 m temperature (T), total precipitation (p), snow depth (h_S), sea surface temperature (T_s)—are drawn from the ERA5 reanalysis (Hersbach et al., 2020), restricted to latitudes poleward of 65°N and averaged to represent the basin mean anomaly. Two fields are weakly constrained over the ice-pack and are interpreted accordingly. T_s is prescribed at the seawater freezing point (~ -1.8°C) beneath ice-covered cells, so its basin-scale variance derives from the open-water and marginal-ice fraction. Additionally, ERA5 snow depth is derived from the HTESSEL scheme (Batrak & Müller, 2019), such that h_S represents large-scale accumulation rather than redistributed snow on sea ice (Wang et al., 2019). Peripheral seas are extracted by basin using the NSIDC region mask and rolling correlations identical to those in Figure 3a are computed within each regional boundary.

3. Results

3.1. Long Term Budget Behavior

Our budget yields a spatially resolved, 29-year record of winter monthly SIV thermodynamic and dynamic terms. Analysis of the budget reveals non-stationary Arctic sea-ice system growth behavior, strongly informed by the spatial heterogeneity of the Arctic sea ice system. We observe a higher production of ice in the Siberian, Laptev and Kara seas relative to the Arctic basin, and a heterogeneous melt and growth pattern on the ice edge (Figure 1). The altimetric record shows a decline in March SIV of 1,943 km^3 (−67 km^3 yr^{-1}) over 1994–2023 (Figure 2a), less than pan-Arctic estimates because the pole-hole excludes the thinning of multiyear ice above 81.5°N. Dynamic contributions of *Adv* and *Div* tend to cancel out, with an ONDJFM net value of −459(±256) km^3. The domain integral does not vanish because both the 81.5°N boundary and the ice edge are open.

We define seasonal growth, Res_{Seas}, as the ONDJFM integral of positive *Res*. Mean seasonal growth is 8,033 km^3, with an inter-annual standard deviation of 771 km^3 and a peak of 9,341 km^3 in 2018. This is lower than pan-Arctic estimates because our domain ends at 81.5°N and our record covers only ONDJFM. Descriptive statistics by growth regime are given in Table S1 in Supporting Information S1. We also identify three regimes in the record of growth (Figure 2a). Mean winter growth volume has increased from the 1994–2002 period mean of 7,336 km^3, an intermediate regime (2002–2007) value of 7,977 km^3, to a step change of growth into a post 2007 mean value of 8,413 km^3, a total change of 1,077 (±259) km^3. To test the significance of the time series change we use Linearly Penalized Segmentation Analysis and a Gaussian kernel, known as the Radial Basis Function (Killick et al., 2012), which identifies the winters of 2002/03 and 2007/08 as regime change points in basin-wide Arctic sea ice growth behavior ($\beta = 0.5$). Key region regime changes are identified over 2002/03 and 2007/08 winters for the Beaufort Chukchi, and Siberian Laptev and Kara regions respectively.

The post 2007 period of heightened growth is characterized by a steeper, and non-linear seasonal growth curve as seen in Figure 2b. October-November growth rates are higher relative to the low-growth (1994–2002) and

10.1029/2026GL125585

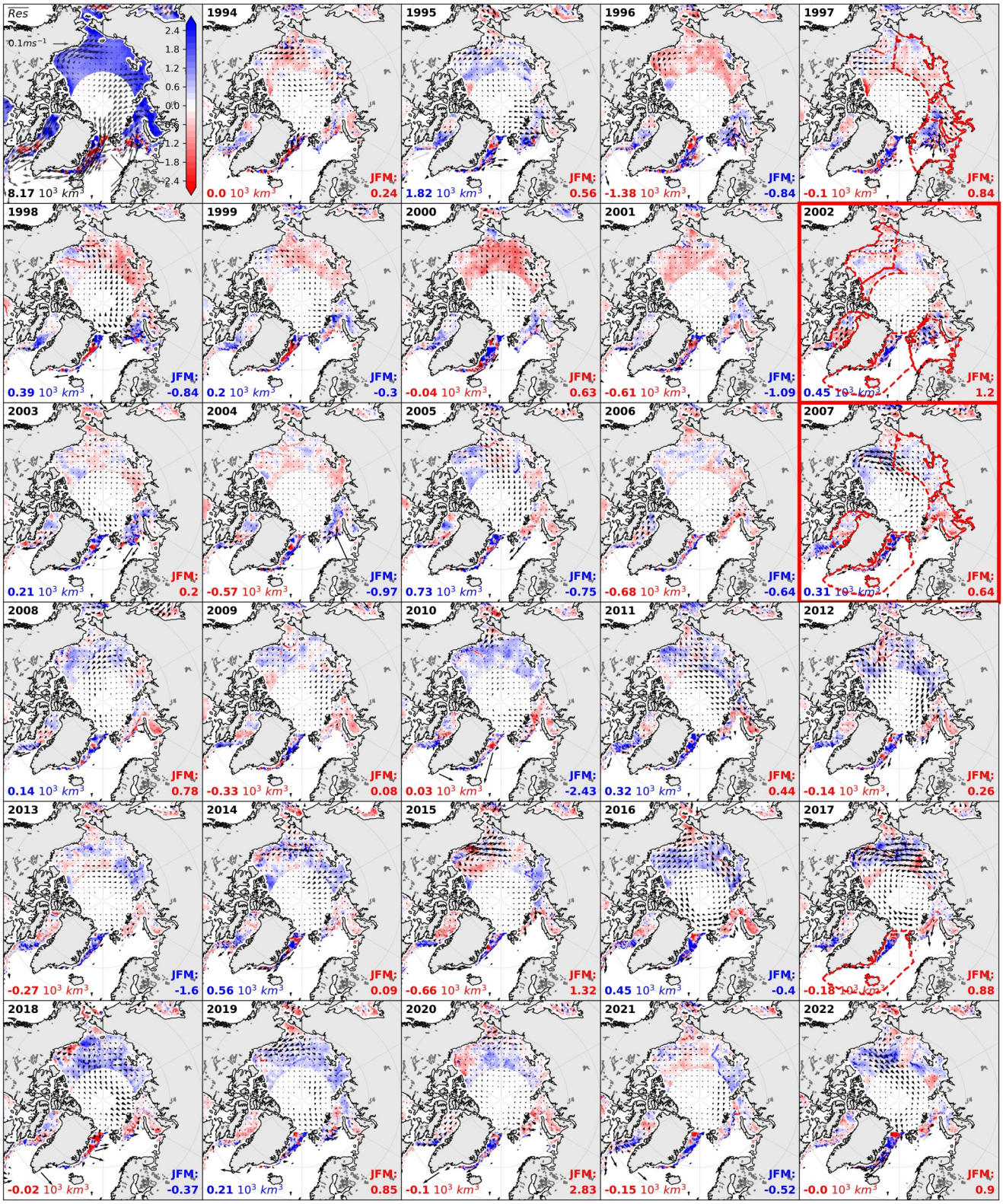


Figure 1. The top left panel shows the climatological mean *Res* and drift. All other panels show the climatological anomaly of *Res* and drift, where bold arrows indicate the 90th percentile drift speed. Subplot annotations include the Arctic ocean basin growth anomaly relative to the low-pass Butterworth filter of Figure 2 (bottom left) and the Jan-Feb-Mar Arctic Oscillation anomaly (bottom right). Region highlights indicate identified regime shifts (PELT, $\beta = 0.5$), (Figure S1 in Supporting Information S1 for NSIDC region map).

19448007, 2026, 22, Downloaded from https://agupubs.onlinelibrary.wiley.com/doi/10.1029/2026GL125585 by NICE, National Institute for Health and Care Excellence, Wiley Online Library on [19/11/2026]. See the Terms and Conditions (https://onlinelibrary.wiley.com/terms-and-conditions) on Wiley Online Library for rules of use; OA articles are governed by the applicable Creative Commons License

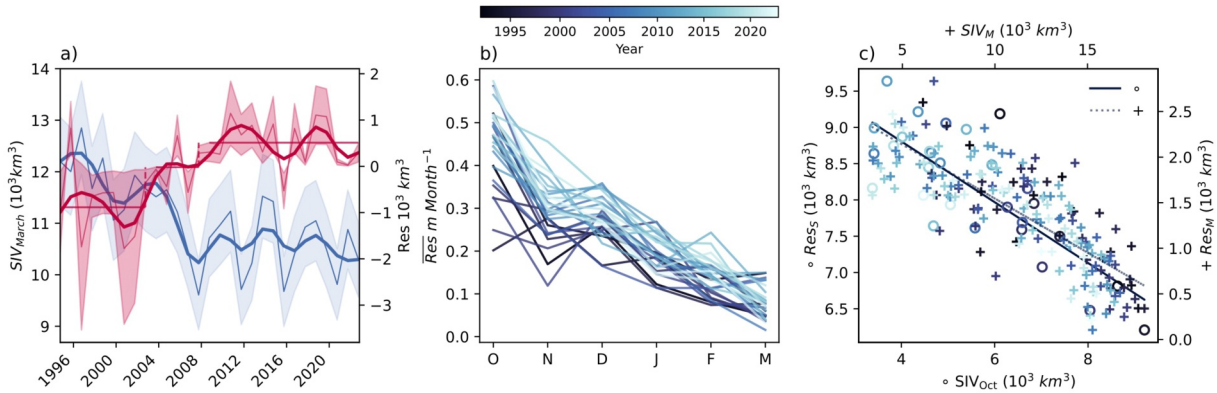


Figure 2. The changing response of Arctic growth over 29 years, represented by (a) the time-series of anomaly *Res* with March sea ice volume (SIV), where horizontal lines mark the period means of the three growth regimes identified by the segmentation, (b) mean residual (growth) per grid cell expressed as an annual curve and (c) the thermodynamic feedback for the Arctic basin, where ∘ shows seasonal integrals are predictable as a function of October SIV $\left(SIV_{\mathrm{Oct}},\ Res_{\mathrm{Seas}},\ p = 3.31 \times 10^{-7},\ r^2 = 0.6250\right)$, and where + represents monthly growth as a function of the initial SIV of the basin for that month $\left(SIV_{\mathrm{Month}} Res_{\mathrm{Month}},\ p = 5.59 \times 10^{-40},\ r^2 = 0.640\right)$.

transition (2003–2007) regimes. The regression of survived summer SIV in October against seasonal *Res* is highly significant ($p = 3.31 \times 10^{-7},\ r^2 = 0.625$) (See Figure 2c). This relationship holds for monthly feedbacks, such that the amount of ice grown in a month is significantly negatively related to the initial monthly volume conditions ($p = 5.59 \times 10^{-40},\ r^2 = 0.64$). The strength of the feedback is only marginally altered by the inclusion of data up to 88°N for the CS2 era, such that the change in correlation for the 10-year period from 2010 to 2020 is $-0.083(-0.369, 0.184)$, see Section S4 in Supporting Information S1. By performing 10-year rolling correlations of $\rho(SIV_{\mathrm{Month}},\ Res_{\mathrm{Seas}})$ bootstrapped 2,000 times for the basin and regional seas, we investigate the stationarity of the negative volume feedback.

Figure 3a demonstrates that post 2007 thickness regime shift, ONDJFM growth becomes decoupled from the initial volume conditions. The strongest relationship reverses from $\rho(SIV_{\mathrm{Oct}},\ Res_{\mathrm{Seas}})$ into $\rho(Res_{\mathrm{Seas}}, SIV_{\mathrm{March}})$. After 2007 a growing share of the March volume consists of ice formed during the preceding winter. This relationship is informed by regional sea behavior. The Beaufort and Chukchi observe the inversion of the relationship based on the observed growth curve regime shift of 2002, but the Siberian, Laptev and Kara seas demonstrate a weaker and later decoupling around the respective shift in 2007 (Figures 3b and 3d). The Central Arctic basin retains a negative feedback that weakens through the 2000s and re-emerges after 2012 ($R \approx -0.4$), while the Barents Sea shows a persistent positive relationship ($R > 0.6$).

3.2. Atmospheric Interactions

Across the record, the Arctic sea ice system exhibits non-stationary sensitivity to these drivers, see Figure 3f. T ($R \approx 0.6$), T_s ($R \approx 0.5$), and p ($R \approx 0.5$) are positively coupled and h_S ($R \approx -0.6$) negatively coupled to ice growth prior to the 2007 regime shift. After 2007, the correlations become predominantly statistically insignificant for approximately 15 years. Thus, the interval during which initial volume conditions exert a significant influence on growth coincides with periods of enhanced coupling between reanalysis fields and growth. However, the ice–atmosphere decoupling identified over the 2010s may be inverting: T exhibits a trend toward a strongly negative association with the seasonal residual.

Prior to 2007, the Beaufort, Chukchi, Siberian, Laptev, and Kara seas exhibit coupling patterns that are closely reflected in the basin-scale integral metric (Figures 3g and 3i). Moreover, the aforementioned temperature sensitivity is dominated by coupling between sea-ice growth in the Siberian, Laptev, and Kara seas and surface air temperature of $R \approx -0.5$ (Figure 3i). In contrast, sea-ice growth in the central Arctic shows no statistically significant relationship with the reanalysis variables over the full observational period. The Barents Sea (Figure 3j), however, displays a strong negative coupling with both T ($R \approx -0.5$) and T_s ($R \approx -0.5$), a weaker yet distinct relationship with p ($R \approx -0.3$), and a positive coupling with h_s ($R \approx 0.5$).

19448007, 2026, 22, Downloaded from https://agupubs.onlinelibrary.wiley.com/doi/10.1029/2026GL125585 by NICE, National Institute for Health and Care Excellence, Wiley Online Library on [19/11/2026]. See the Terms and Conditions (https://onlinelibrary.wiley.com/terms-and-conditions) on Wiley Online Library for rules of use; OA articles are governed by the applicable Creative Commons License

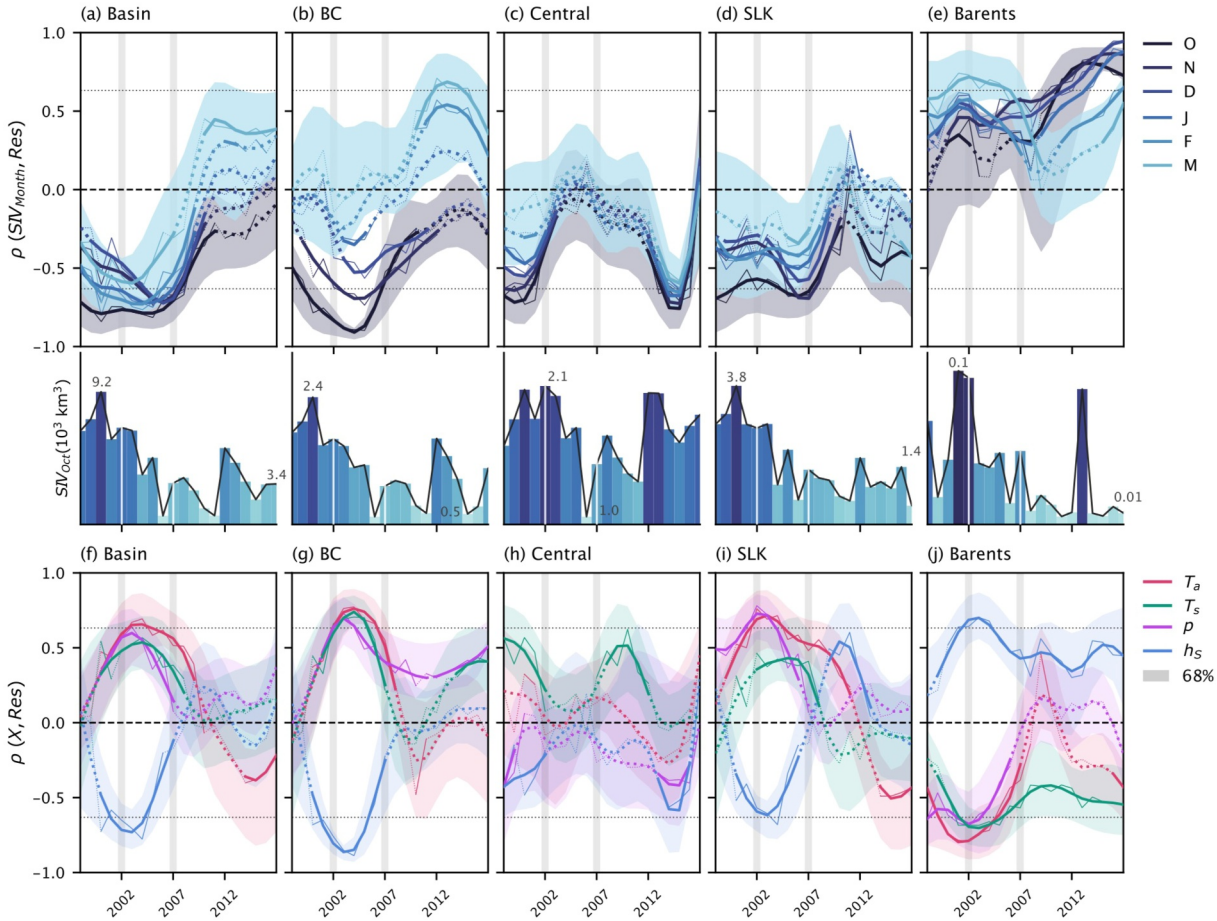


Figure 3. 10 years rolling correlations for Arctic regions. Plots (a–e) are the $SIV_{\text{Month}} \rightarrow Res_{\text{Seas}}$ with October sea ice volume (10^3 km^3, shading is bootstrapping for SIV_{Oct} and SIV_{March} relationships, regionally scaled) beneath. Plots (f–j) are the reanalysis variables T_a–2 m air temperature, T_s–sea surface temperature, p–total precipitation, h_S–height of snow $\rightarrow Res_{\text{Seas}}$. Insignificant correlations below the 90th percentile are dotted lines, shading are bootstrapped 2,000 times and plotted to the 95% significance threshold. Gray vertical bands are the 2002/03 and 2007/08 PELT changepoints.

4. Discussion and Conclusion

By decomposing a 29-year (1994–2023) pan-Arctic SIV budget into dynamic and thermodynamic components, we identify an upward regime shift in winter growth behavior centered on the winter of 2007–2008. The shift marks the collapse of the negative volume feedback that governed late twentieth-century growth and the emergence of a thinner, more internally variable pack whose growth is largely decoupled from atmospheric forcing.

Our volume budget resolves three growth regimes: low-growth (1994–2002), transition (2003–2007), and high intensity growth (2007 onwards). Previous Arctic SIV budgets have started at later dates (Heorton et al., 2025; Ricker et al., 2021), and thus have been unable to resolve the low-growth regime. The final transition matches the extent and thickness regime shifts of Stern (2025) and Sumata et al. (2023). Those studies identify shifts from sea ice state (SIC or SIT); here for the first time, we characterize regimes directly through the process of sea ice growth. In this framing the shift is a step-change in mean winter growth of 1,077 (±259) km^3, driven by a steeper, non-linear October–November dominant growth curve, consistent with model representations that resolve thin-ice growth feedbacks (Massonnet et al., 2018). Both transitions occurred at modest global-mean temperature anomalies of +0.54°C (2002) and +0.59°C (2007) (Morice et al., 2021).

Through the twentieth and early twenty-first centuries, winter growth was controlled by a strong negative volume feedback: thicker October ice suppressed subsequent growth (Hibler, 1979). Growth also correlated with air temperature, sea surface temperature, precipitation and snow depth, but these couplings, like the volume

19448007, 2026, 22, Downloaded from https://agupubs.onlinelibrary.wiley.com/doi/10.1029/2026GL125585 by NICE, National Institute for Health and Care Excellence, Wiley Online Library on [19/11/2026]. See the Terms and Conditions (https://onlinelibrary.wiley.com/terms-and-conditions) on Wiley Online Library for rules of use; OA articles are governed by the applicable Creative Commons License

19448007, 2026, 22, Downloaded from https://agupubs.onlinelibrary.wiley.com/doi/10.1029/2026GL125585 by NICE, National Institute for Health and Care Excellence, Wiley Online Library on [19/11/2026]. See the Terms and Conditions (https://onlinelibrary.wiley.com/terms-and-conditions) on Wiley Online Library for rules of use; OA articles are governed by the applicable Creative Commons License

feedback, are set by SIV itself, the reanalysis couplings are not independent controls on growth. Two observations support this conclusion. First, warm and wet years grew more ice ($R \approx 0.5$ to 0.6; Figure 3f), whereas warmer air, a warmer ocean and more snowfall should each slow growth. Warm years were thin-ice years, and thin ice under thin snow conducts more heat, so grows faster (Bigdeli et al., 2020; Petty et al., 2018). Second, the timing is important as all four couplings weaken after 2007 alongside the negative volume feedback. Independent controls should have strengthened as the pack thinned (Petty et al., 2018). Only air temperature re-emerges, at $R \approx -0.5$ since 2014 and only regionally (Figure 3i). If anything, growth responds to the confluence of forcings rather than to a single index (Swart et al., 2015).

A thinner, more homogeneous pack held near ∼1.5 m (Sumata et al., 2023) no longer supplies the thickness variance the conductive feedback converts into growth variance. The sea-ice pack now occupies an intermediate state that is too thin and too homogeneous to sustain the conductive feedback relationship, yet too thick for atmospheric anomalies to set growth at the basin scale. Enhanced variability and weakened control under intermediate-thickness conditions were anticipated by Goosse et al. (2009), who place the maximum-variance sea-ice extent state where winter thickness falls between 1.24 and 2.33 m; the present pack lies within that range (Sumata et al., 2023). A similar internally variable outcome is anticipated for an Arctic in which seasonal memory is lost to summer melt (Notz & Stroeve, 2018). Our observations thus demonstrate a regime where growth is consequently high, near-uniform and weakly determined by either volume or reanalysis predictors, that has been sustained for 17 years.

Ricker et al. (2021) observe the same feedback regionally from 2002 to 2019, finding significant anti-correlation between initial volume condition and growth in the East Siberian and Laptev seas, but not in the Barents and Kara where oceanic heat flux and surface temperature dominate. Their domain is bounded at 81.0°N and their record begins in 2002, within our transition period, so they resolve a mean relationship rather than a change. However, Ricker et al. (2021) project a weakening of the negative feedback as a consequence of a first year ice dominated ice pack. Our study shows the weakening occurs from 2002 to 2007. This is likely due to differences in methodologies employed: first Ricker et al. (2021) begin their analysis within the observed transition period and second, our budgets are computed in different ways. Ricker et al. (2021) take regional growth as the residual of volume change and the flux through a region's boundaries, whereas we compute the residual at each grid cell, and the open 81.5°N boundary and ice edge enter only the domain-integrated dynamic term. Over the CS2 era Heorton et al. (2025) used the same grid-cell volume budget as this study, extended to 88°N, and find no consistent Arctic-wide negative volume feedback. In fact, they report lower winter growth in years of anomalously low volume (2013, 2016, 2018), the opposite expected under an active volume feedback. Heorton et al. (2025) attribute variation in growth largely to drift anomaly rather than thermodynamic forcing. This is the expected result in a homogeneous, high-intensity growth regime.

Over 2015–2023 CESM-LE projects an October thickness–seasonal growth correlation of $R \approx -0.85$ (Petty et al., 2018, their Figure 4a). The October volume anomaly is predominantly thickness anomaly, and over the same period we observe $\rho(SIV_{\mathrm{Oct}}, Res_{\mathrm{Seas}}) = -0.30$, bounded between −0.75 and 0.15, which excludes the projected value. Petty et al. (2018) find that these inversions occur as ocean domains become seasonally ice-free, so the projected inversion marks the point at which growth ceases to be conductive-flux limited and becomes limited by ice–ocean–atmosphere fluxes. Our observations support Petty et al. (2018)'s interpretation, but not the timing. However, the domains are not identical, as Petty et al. (2018) impose no pole-hole, so their analysis includes the Last Ice Area. Due to the pole-hole we have excluded a cap of 2.7×10^6 km^2 that holds a disproportionate share of the remaining multiyear ice. Radar altimetry coverage of the cap begins with CryoSat-2, so the transitions predate observation of this region; its exclusion can therefore bias the magnitude of the correlations but not the dates at which they happen. Reducing the pole-hole by including the sea-ice up to 88°N over the CryoSat-2 era changes the correlation by −0.083 (−0.369, 0.184). This is a non-negligible amount, but not enough to restore the pre-2007 feedback strength. The pole-hole's variance share bounds its possible contribution to the Arctic-wide feedback (Section S4 in Supporting Information S1), and would not be strong enough to affect our interpretation of feedback collapse.

The Arctic sea ice system has therefore left the volume feedback regime around the record decline year of 2007, without entering the atmosphere–ocean forced regime expected to succeed it. Across CMIP6 the projected turnover from basal growth spans the 2020s to the 2080s, and is largely set by each model's rate of winter ice loss

19448007, 2026, 22, Downloaded from https://agupubs.onlinelibrary.wiley.com/doi/10.1029/2026GL125585 by NICE, National Institute for Health and Care Excellence, Wiley Online Library on [19/11/2026]. See the Terms and Conditions (https://onlinelibrary.wiley.com/terms-and-conditions) on Wiley Online Library for rules of use; OA articles are governed by the applicable Creative Commons License

(Keen et al., 2021). Our transition sits before the beginning of the CMIP6 range of dates. CESM-LE's sea ice module is CICE4 (Kay et al., 2015), so comparable behavior might be expected of other CICE4-driven models that use the Bitz-Lipscomb scheme; in CMIP6, schemes that use the mushy-layer formation produce less growth (Keen et al., 2021), and a similar mushy-layer scheme is introduced to CICE5 (Bailey et al., 2020). The projected feedback is not independent of the thermodynamic scheme. Our interpretation rests on a single ensemble under RCP8.5, but the CMIP6 spread in March ice mass, 13–29 $\times$ 10^3 Gt against 16–20 $\times$ 10^3 Gt in PIOMAS (Keen et al., 2021), is three times larger than the reanalysis range. A multi-model comparison would therefore resolve mean-state bias rather than feedback behavior. As such, a direct and systematic treatment awaits CMIP7 (Fox-Kemper et al., 2026).

The Central Arctic and Barents Sea represent the two extremes of growth behavior. The Central Arctic has a varied negative volume-growth feedback across the record ($R \approx -0.4$), a reflection of its dynamically driven volume and limited atmospheric sensitivity, and can be thought of analogously to the Arctic basin before 2007. The feedback re-emerges as Central Arctic volume increases, though we interpret this cautiously because of the pole-hole limitation (Section 2.1). The Barents, by contrast, exhibits positive volume state-dependency and a strong negative coupling to sea surface temperature ($R \approx -0.5$) throughout. Driven by proximity to Atlantic water inflow, open-ocean heat exchange and thinner ice (Barton et al., 2018), control of growth in the Barents has turned over from volume to temperature (Docquier & Koenigk, 2021), and this domain thus supports the terminal decline of the European sector observed by Ricker et al. (2021). The Barents could therefore be considered the future state of Arctic sea ice, and *Atlantification* the transition to it; we find the wider basin is not yet in that highly sensitive mode, but in a distinct, intermediate state. The peripheral seas are where this distinction is likely to break down first. The re-emergence of temperature coupling across the Siberian, Laptev and Kara seas in the 2010s (Figure 3i) marks them as the most atmospherically sensitive components of the present regime, Barents aside. The inclusion of the pole-hole up to 88°N does not significantly alter the Arctic ocean negative volume feedback correlation for the CS2 era (Section S4 in Supporting Information S1), and is consistent with our broader interpretation of pack homogenization and thinning that collapses $\rho(SIV_{\mathrm{Oct}}, Res)$.

Across both growth regimes, October SIV is the most robust predictor of seasonal growth $\left(r^2 = 0.625\right)$, outperforming SIC $\left(r^2 = 0.36\right)$ (Figure S6 in Supporting Information S1). Concentration alone cannot capture the thickness distribution that governs conductive flux and, consequently, growth rate. The relative weakness of SIC as a predictor reflects the importance of metric selection when characterizing the sea ice state (Fox-Kemper et al., 2026; Meier & Stroeve, 2022). This motivates the use of SIV as the governing variable in both observational and model-based assessments. The choice of metric affects what a regime shift looks like and when it becomes observable. Monitoring volume production in the atmospherically sensitive peripheral seas is likely to give the earliest observational signal of an incipient transition toward seasonally ice-free conditions (Hankel & Tziperman, 2023; Jahn et al., 2024).

5. Future Work

This study is limited by data availability, not method. The budget framework extends to the melt season because year-round freeboard retrievals enable summer SIT estimates (Heorton et al., 2025; Landy et al., 2022), and to new thickness products that improve interpolation poleward of 81.5°N. Beyond sea ice, volume budgeting also offers a method to constraining surface freshwater source terms (Haumann et al., 2016) and freshwater fluxes that link growth and melt to biological systems (Boetius et al., 2015; Dieckmann & Hellmer, 2003). Our results identify a growth regime that CESM-LE under RCP8.5 does not reproduce. It is governed by internal variability and the basin thickness distribution, not by a dominant ice–ocean–atmosphere forcing. This volume budget provides the observational benchmark against which CMIP7 can be tested across distinct growth regimes (Fox-Kemper et al., 2026), and reframes SIV as the variable that governs and reveals Arctic growth behavior.

Conflict of Interest

The authors declare no conflicts of interest relevant to this study.

Availability Statement

Budget methodology code can be found here https://github.com/CPOMUCL/Budget_tool (Heorton et al., 2025), and the Bocquet et al. (2024) thickness https://zenodo.org/records/12783561, concentration https://www.ncei.noaa.gov/products/climate-data-records/sea-ice-concentration (Cavalieri et al., 1984, 1997), OSISAF-405 https://osi-saf.eumetsat.int/products/osi-405-d and Pathfinder v4 https://nsidc.org/data/nsidc-0116/versions/4 (Lavergne & Down, 2023; Tschudi et al., 2020). Both Pathfinder v4 and OSISAF-405 derived budget outputs can be found in this repository https://doi.org/10.5281/zenodo.19481416 (Mellor et al., 2026). ERA5 global reanalysis is made available at this address https://cds.climate.copernicus.eu/datasets/reanalysis-era5-single-levels-monthly-means (Hersbach et al., 2020).

Acknowledgments
B.M. and C.B. acknowledge support from NERC training Grant (NE/S007229/1). M. T. was supported by UKRI Natural Environment Research Council (NERC) through the Correcting Seasonal Feedbacks for Physically Constrained Sea Ice Reanalysis (CRiSP) project (Grant UKRI9274); by the Advanced Research and Invention Agency (ARIA) through the Re-thickening Arctic Sea Ice (RASI) project, part of the Exploring Climate Cooling programme (Grant G941562); and by the European Space Agency through the SIN'XS project (contract NOV-FE-1291-CT-013).

References

Bailey, D. A., Holland, M. M., DuVivier, A. K., Hunke, E. C., & Turner, A. K. (2020). Impact of a new sea ice thermodynamic formulation in the CESM2 sea ice component. *Journal of Advances in Modeling Earth Systems*, *12*(11), e2020MS002154. https://doi.org/10.1029/2020MS002154

Barton, B. I., Lenn, Y.-D., & Lique, C. (2018). Observed atlantification of the Barents Sea causes the polar front to limit the expansion of winter sea ice. *Journal of Physical Oceanography*, *48*(8), 1849–1866. https://doi.org/10.1175/JPO-D-18-0003.1

Batrak, Y., & Müller, M. (2019). On the warm bias in atmospheric reanalyses induced by the missing snow over arctic sea-ice. *Nature Communications*, *10*(1), 4170. https://doi.org/10.1038/s41467-019-11975-3

Bigdeli, A., Nguyen, A. T., Pillar, H. R., Ocaña, V., & Heimbach, P. (2020). Atmospheric warming drives growth in arctic sea ice: A key role for snow. *Geophysical Research Letters*, *47*(20), e2020GL090236. https://doi.org/10.1029/2020GL090236

Bitz, C. M., & Roe, G. H. (2004). A mechanism for the high rate of sea ice thinning in the Arctic Ocean. *Journal of Climate*, *17*(18), 3623–3632. https://doi.org/10.1175/1520-0442(2004)017⟨3623:AMFTHR⟩2.0.CO;2

Bocquet, M., Fleury, S., Piras, F., Rinne, E., Sallila, H., Garnier, F., & Rémy, F. (2023). Arctic sea ice radar freeboard retrieval from the European remote-sensing satellite (ERS-2) using altimetry: Toward sea ice thickness observation from 1995 to 2021. *The Cryosphere*, *17*(7), 3013–3039. https://doi.org/10.5194/tc-17-3013-2023

Bocquet, M., Fleury, S., Rémy, F., & Piras, F. (2024). Arctic and Antarctic sea ice thickness and volume changes from observations between 1994 and 2023. *Journal of Geophysical Research: Oceans*, *129*(11), e2023JC020848. https://doi.org/10.1029/2023JC020848

Boetius, A., Anesio, A. M., Deming, J. W., Mikucki, J. A., & Rapp, J. Z. (2015). Microbial ecology of the cryosphere: Sea ice and glacial habitats. *Nature Reviews Microbiology*, *13*(11), 677–690. https://doi.org/10.1038/nrmicro3522

Cavalieri, D. J., Gloersen, P., & Campbell, W. J. (1984). Determination of sea ice parameters with the NIMBUS 7 SMMR. *Journal of Geophysical Research*, *89*(D4), 5355–5369. https://doi.org/10.1029/JD089iD04p05355

Cavalieri, D. J., Parkinson, C. L., Gloersen, P., & Zwally, H. J. (1997). *Arctic and Antarctic sea ice concentrations from multichannel passive-microwave satellite data sets: October 1978–September 1995 user's guide (NASA technical memorandum no. 104647)*. NASA Goddard Space Flight Center. Retrieved from https://ntrs.nasa.gov/citations/19980076134

Dawson, G., Landy, J., Tsamados, M., Komarov, A. S., Howell, S., Heorton, H., & Krumpen, T. (2022). A 10-year record of arctic summer sea ice freeboard from cryosat-2. *Remote Sensing of Environment*, *268*, 112744. https://doi.org/10.1016/j.rse.2021.112744

Dieckmann, G. S., & Hellmer, H. H. (2003). The importance of sea ice: An overview. Sea ice: An introduction to its physics. *Chemistry, Biology and Geology*, 1–21. https://doi.org/10.1002/9780470757161.ch1

Docquier, D., & Koenigk, T. (2021). A review of interactions between ocean heat transport and arctic sea ice. *Environmental Research Letters*, *16*(12), 123002. https://doi.org/10.1088/1748-9326/ac30be

Edel, L., Claud, C., Genthon, C., Palerme, C., Wood, N., L'Ecuyer, T., & Bromwich, D. (2020). Arctic snowfall from cloudsat observations and reanalyses. *Journal of Climate*, *33*(6), 2093–2109. https://doi.org/10.1175/JCLI-D-19-0105.1

England, M. R., Polvani, L. M., Screen, J., & Chan, A. C. (2025). Minimal arctic sea ice loss in the last 20 years, consistent with internal climate variability. *Geophysical Research Letters*, *52*(15), e2025GL116175. https://doi.org/10.1029/2025GL116175

Fox-Kemper, B., DeRepentigny, P., Treguier, A. M., Stepanek, C., O'Rourke, E., Mackallah, C., et al. (2026). CMIP7 data request: Ocean and sea ice priorities and opportunities. *Geoscientific Model Development*, *19*(13), 6043–6078. https://doi.org/10.5194/gmd-19-6043-2026

Gascard, J.-C., Zhang, J., & Rafizadeh, M. (2019). Rapid decline of arctic sea ice volume: Causes and consequences. *The Cryosphere Discussions*, *2019*, 1–29. https://doi.org/10.5194/tc-2019-2

Goosse, H., Arzel, O., Bitz, C. M., de Montety, A., & Vancoppenolle, M. (2009). Increased variability of the arctic summer ice extent in a warmer climate. *Geophysical Research Letters*, *36*(23). https://doi.org/10.1029/2009GL040546

Hankel, C., & Tziperman, E. (2023). An approach for projecting the timing of abrupt winter arctic sea ice loss. *Nonlinear Processes in Geophysics*, *30*(3), 299–309. https://doi.org/10.5194/npg-30-299-2023

Haumann, F. A., Gruber, N., Münnich, M., Frenger, I., & Kern, S. (2016). Sea-ice transport driving southern ocean salinity and its recent trends. *Nature*, *537*(7618), 89–92. https://doi.org/10.1038/nature19101

Hendricks, S., Ricker, R., & Paul, S. (2021). Product user guide and algorithm specification: AWI cryosat-2 sea ice thickness (version 2. 4). *EPIC3*. Retrieved from https://epic.awi.de/id/eprint/54733/

Heorton, H., Tsamados, M., Landy, J., & Holland, P. R. (2025). Observationally constrained estimates of the annual arctic sea-ice volume budget 2010–2022. *Annals of Glaciology*, *66*, e9. https://doi.org/10.1017/aog.2025.3

Hersbach, H., Bell, B., Berrisford, P., Hirahara, S., Horányi, A., Muñoz-Sabater, J., et al. (2020). The ERA5 global reanalysis. *The Quarterly Journal of the Royal Meteorological Society*, *146*(730), 1999–2049. https://doi.org/10.1002/qj.3803

Hibler, W., III. (1979). A dynamic thermodynamic sea ice model. *Journal of Physical Oceanography*, *9*(4), 815–846. https://doi.org/10.1175/1520-0485(1979)009⟨0815:ADTSIM⟩2.0.CO;2

Jahn, A., Holland, M. M., & Kay, J. E. (2024). Projections of an ice-free arctic ocean. *Nature Reviews Earth and Environment*, *5*(3), 164–176. https://doi.org/10.1038/s43017-023-00515-9

Kay, J. E., Deser, C., Phillips, A., Mai, A., Hannay, C., Strand, G., et al. (2015). The community earth system model (CESM) large ensemble project: A community resource for studying climate change in the presence of internal climate variability. *Bulletin of the American Meteorological Society*, *96*(8), 1333–1349. https://doi.org/10.1175/BAMS-D-13-00255.1

19448007, 2026, 22, Downloaded from https://agupubs.onlinelibrary.wiley.com/doi/10.1029/2026GL125585 by NICE, National Institute for Health and Care Excellence, Wiley Online Library on [19/11/2026]. See the Terms and Conditions (https://onlinelibrary.wiley.com/terms-and-conditions) on Wiley Online Library for rules of use; OA articles are governed by the applicable Creative Commons License

Keen, A., Blockley, E., Bailey, D. A., Boldingh Debernard, J., Bushuk, M., Delhaye, S., et al. (2021). An inter-comparison of the mass budget of the arctic sea ice in CMIP6 models. *The Cryosphere*, *15*(2), 951–982. https://doi.org/10.5194/tc-15-951-2021

Kern, S., Lavergne, T., Notz, D., Pedersen, L. T., Tonboe, R. T., Saldo, R., & Sørensen, A. M. (2019). Satellite passive microwave sea-ice concentration data set intercomparison: Closed ice and ship-based observations. *The Cryosphere*, *13*(12), 3261–3307. https://doi.org/10.5194/tc-13-3261-2019

Killick, R., Fearnhead, P., & Eckley, I. A. (2012). Optimal detection of changepoints with a linear computational cost. *Journal of the American Statistical Association*, *107*(500), 1590–1598. https://doi.org/10.1080/01621459.2012.737745

Kwok, R. (2010). Satellite remote sensing of sea-ice thickness and kinematics: A review. *Journal of Glaciology*, *56*(200), 1129–1140. https://doi.org/10.3189/002214311796406167

Landy, J. C., Dawson, G. J., Tsamados, M., Bushuk, M., Stroeve, J. C., Howell, S. E. L., et al. (2022). A year-round satellite sea-ice thickness record from CryoSat-2. *Nature*, *609*(7927), 517–522. https://doi.org/10.1038/s41586-022-05058-5

Landy, J. C., Petty, A. A., Tsamados, M., & Stroeve, J. C. (2020). Sea ice roughness overlooked as a key source of uncertainty in cryosat-2 ice freeboard retrievals. *Journal of Geophysical Research: Oceans*, *125*(5), e2019JC015820. https://doi.org/10.1029/2019JC015820

Lang, A., Yang, S., & Kaas, E. (2017). Sea ice thickness and recent Arctic warming. *Geophysical Research Letters*, *44*(1), 409–418. https://doi.org/10.1002/2016GL071274

Lavergne, T., & Down, E. (2023). A climate data record of year-round global sea-ice drift from the EUMETSAT ocean and sea ice satellite application facility (Osi saf). *Earth System Science Data*, *15*(12), 5807–5834. https://doi.org/10.5194/essd-15-5807-2023

Lim, W.-I., Park, H.-S., Stewart, A. L., & Seo, K.-H. (2022). Suppression of arctic sea ice growth in the Eurasian–pacific seas by winter clouds and snowfall. *Journal of Climate*, *35*(2), 669–686. https://doi.org/10.1175/JCLI-D-21-0282.1

Mackie, S., Langhorne, P. J., Heorton, H. D., Smith, I. J., Feltham, D. L., & Schroeder, D. (2020). Sea ice formation in a coupled climate model including grease ice. *Journal of Advances in Modeling Earth Systems*, *12*(8), e2020MS002103. https://doi.org/10.1029/2020MS002103

Massonnet, F., Vancoppenolle, M., Goosse, H., Docquier, D., Fichefet, T., & Blanchard-Wrigglesworth, E. (2018). Arctic sea-ice change tied to its mean state through thermodynamic processes. *Nature Climate Change*, *8*(7), 599–603. https://doi.org/10.1038/s41558-018-0204-z

Meier, W. N., & Stroeve, J. (2022). An updated assessment of the changing arctic sea ice cover. *Oceanography*, *35*(3/4), 10–19. https://doi.org/10.5670/oceanog.2022.114

Mellor, B., Tsamados, M., Heorton, H., Holland, P., & Brierley, C. (2026). Sea ice volume budgets 1994–2023 (version 1) [Dataset]. *Zenodo*. https://doi.org/10.5281/zenodo.19481416

Morice, C. P., Kennedy, J. J., Rayner, N. A., Winn, J. P., Hogan, E., Killick, R. E., et al. (2021). An updated assessment of near-surface temperature change from 1850: The hadcrut5 data set. *Journal of Geophysical Research: Atmospheres*, *126*(3), e2019JD032361. https://doi.org/10.1029/2019JD032361

Nab, C., Mallett, R., Gregory, W., Landy, J., Lawrence, I., Willatt, R., et al. (2023). Synoptic variability in satellite altimeter-derived radar freeboard of arctic sea ice. *Geophysical Research Letters*, *50*(2), e2022GL100696. https://doi.org/10.1029/2022GL100696

Nakawo, M., & Sinha, N. K. (1981). Growth rate and salinity profile of first-year sea ice in the high arctic. *Journal of Glaciology*, *27*(96), 315–330. https://doi.org/10.3189/S0022143000015409

Notz, D., & Bitz, C. M. (2017). Sea ice in Earth system models. In D. N. Thomas (Ed.), *Sea ice* (1st ed., pp. 304–325). Wiley. https://doi.org/10.1002/9781118778371.ch12

Notz, D., & Stroeve, J. (2018). The trajectory towards a seasonally ice-free arctic ocean. *Current Climate Change Reports*, *4*(4), 407–416. https://doi.org/10.1007/s40641-018-0113-2

Petty, A. A., Holland, M. M., Bailey, D. A., & Kurtz, N. T. (2018). Warm arctic, increased winter sea ice growth? *Geophysical Research Letters*, *45*(23). https://doi.org/10.1029/2018GL079223

Pollock, M., Diamond, R., Heorton, H., Sime, L., Schroeder, D., & Brierley, C. (2026). An arctic sea ice energy budget for the last interglacial. *Geophysical Research Letters*, *53*(6), e2025GL120781. https://doi.org/10.1029/2025GL120781

Rampal, P., Weiss, J., & Marsan, D. (2009). Positive trend in the mean speed and deformation rate of Arctic sea ice, 1979–2007. *Journal of Geophysical Research*, *114*(C5), 2008JC005066. https://doi.org/10.1029/2008JC005066

Ricker, R., Kauker, F., Schweiger, A., Hendricks, S., Zhang, J., & Paul, S. (2021). Evidence for an increasing role of ocean heat in arctic winter sea ice growth. *Journal of Climate*, *34*(13), 5215–5227. https://doi.org/10.1175/JCLI-D-20-0848.1

Screen, J. A., & Simmonds, I. (2012). Declining summer snowfall in the Arctic: Causes, impacts and feedbacks. *Climate Dynamics*, *38*(11), 2243–2256. https://doi.org/10.1007/s00382-011-1105-2

Serreze, M. C. (2011). Rethinking the sea-ice tipping point. *Nature*, *471*(7336), 47–48. https://doi.org/10.1038/471047a

Stern, H. L. (2025). Regime shift in Arctic Ocean sea-ice extent. *Geophysical Research Letters*, *52*(8), e2024GL114546. https://doi.org/10.1029/2024GL114546

Stroeve, J., Schroder, D., Tsamados, M., & Feltham, D. (2018). Warm winter, thin ice? *The Cryosphere*, *12*(5), 1791–1809. https://doi.org/10.5194/tc-12-1791-2018

Stroeve, J., Serreze, M., Drobot, S., Gearheard, S., Holland, M., Maslanik, J., et al. (2008). Arctic sea ice extent plummets in 2007. *EOS Transactions of the American Geophysical Union*, *89*(2), 13–14. https://doi.org/10.1029/2008EO020001

Sumata, H., de Steur, L., Divine, D. V., Granskog, M. A., & Gerland, S. (2023). Regime shift in Arctic Ocean sea ice thickness. *Nature*, *615*(7952), 443–449. https://doi.org/10.1038/s41586-022-05686-x

Swart, N. C., Fyfe, J. C., Hawkins, E., Kay, J. E., & Jahn, A. (2015). Influence of internal variability on arctic sea-ice trends. *Nature Climate Change*, *5*(2), 86–89. https://doi.org/10.1038/nclimate2483

Tschudi, M. A., Meier, W. N., & Stewart, J. S. (2020). An enhancement to sea ice motion and age products at the national snow and ice data center (NSIDC). *The Cryosphere*, *14*(5), 1519–1536. https://doi.org/10.5194/tc-14-1519-2020

Von Albedyll, L., Hendricks, S., Grodofzig, R., Krumpen, T., Arndt, S., Belter, H. J., et al. (2022). Thermodynamic and dynamic contributions to seasonal Arctic sea ice thickness distributions from airborne observations. *Elementa: Science of the Anthropocene*, *10*(1), 00074. https://doi.org/10.1525/elementa.2021.00074

Wang, C., Graham, R. M., Wang, K., Gerland, S., & Granskog, M. A. (2019). Comparison of ERA5 and era-interim near-surface air temperature, snowfall and precipitation over arctic sea ice: Effects on sea ice thermodynamics and evolution. *The Cryosphere*, *13*(6), 1661–1679. https://doi.org/10.5194/tc-13-1661-2019

West, A. E., Collins, M., & Blockley, E. W. (2020). Using arctic ice mass balance buoys for evaluation of modelled ice energy fluxes. *Geoscientific Model Development*, *13*(10), 4845–4868. https://doi.org/10.5194/gmd-13-4845-2020

19448007, 2026, 22, Downloaded from https://agupubs.onlinelibrary.wiley.com/doi/10.1029/2026GL125585 by NICE, National Institute for Health and Care Excellence, Wiley Online Library on [19/11/2026]. See the Terms and Conditions (https://onlinelibrary.wiley.com/terms-and-conditions) on Wiley Online Library for rules of use; OA articles are governed by the applicable Creative Commons License

Willatt, R., Stroeve, J., Nandan, V., Newman, T., Mallett, R., Hendricks, S., et al. (2023). Retrieval of snow depth on arctic sea ice from surface-based, polarimetric, dual-frequency radar altimetry. *Geophysical Research Letters*, *50*(20), e2023GL104461. https://doi.org/10.1029/2023GL104461

Winton, M. (2006). Does the arctic sea ice have a tipping point? *Geophysical Research Letters*, *33*(23). https://doi.org/10.1029/2006GL028017

References From the Supporting Information

Fetterer, F., Knowles, K., Meier, W. N., Savoie, M., Windnagel, A., & Stafford, T. (2025). Sea ice index (version 4) [Dataset]. *National Snow and Ice Data Center*. https://doi.org/10.7265/A98X-0F50

19448007, 2026, 22, Downloaded from https://agupubs.onlinelibrary.wiley.com/doi/10.1029/2026GL125585 by NICE, National Institute for Health and Care Excellence, Wiley Online Library on [19/11/2026]. See the Terms and Conditions (https://onlinelibrary.wiley.com/terms-and-conditions) on Wiley Online Library for rules of use; OA articles are governed by the applicable Creative Commons License